Developmental Biology 333 (2009) 186–199

Contents lists available at ScienceDirect

Developmental Biology

journal homepage: www.elsevier.com/developmentalbiology

Rho1 has multiple functions in *Drosophila* wing planar polarity

Jie Yan, Qiuheng Lu, Xiaolan Fang, Paul N. Adler *

Biology Department, Department of Cell Biology, Morphogenesis and Regenerative Medicine Institute and Cancer Center, University of Virginia, Charlottesville, VA 22903, USA

ARTICLE INFO

Article history:
Received for publication 27 April 2009
Revised 23 June 2009
Accepted 24 June 2009
Available online 1 July 2009

Keywords:
Planar polarity
Drosophila
Wing
Rho1
Multiple wing hairs

ABSTRACT

The *frizzled* (*fz*) signaling/signal transduction pathway controls planar cell polarity in both vertebrates and invertebrates. Previous data implicated *Rho1* as a component of the *fz* pathway in *Drosophila* but it was unclear how it functioned. The existence of a G Protein Binding-Formin Homology 3 (GBD-FH3) domain in Multiple Wing Hairs, a downstream component of the pathway suggested that Rho1 might function by binding to and activating Mwh.

We re-examined the role of *Rho1* in wing planar polarity and found that it had multiple functions. Aberrant *Rho1* activity led to changes in the number of hairs formed, changes in cell shape and F-actin and changes in cellular junctions. Experiments that utilized Rho effector loop mutations argued that these phenotypes were mediated by effects of Rho1 on the cytoskeleton and not by effects on transcription. We found strong positive genetic interactions between *Rho1* and *mwh*, that *Rho1* regulated the accumulation of Mwh protein and that these two proteins could be co-immunoprecipitated. The Mwh GBD:FH3 domain was sufficient for co-immunoprecipitation with Rho1, consistent with this domain mediating the interaction. However, further experiments showed that Rho1 function in wing differentiation was not limited to interacting with Mwh. We established by genetic experiments that *Rho1* could influence hair morphogenesis in the absence of *mwh* and that the disruption of *Rho1* activity could interfere with the zig zag accumulation pattern of upstream *fz* pathway proteins. Thus, our results argue that in addition to its interaction with Mwh *Rho1* has functions in wing planar polarity that are parallel to and upstream of *fz*. The upstream function may be an indirect one and associated with the requirement for normal apical basal polarity and adherens junctions for the accumulation of PCP protein complexes.

© 2009 Elsevier Inc. All rights reserved.

Introduction

In multicellular animals many cells are polarized in the plane of a tissue. This tissue planar polarity is often obvious in the epidermis and is a property of both the tissue as a whole and of individual cells. Planar cell polarity (PCP) in *Drosophila* is under the control of the *frizzled* (*fz*) signaling pathway (Lawrence et al., 2007; Wong and Adler, 1993; Zallen, 2007). This pathway is widely conserved and functions during gastrulation in vertebrate embryos, during the differentiation of stereocilia in the inner ear and in the mammalian epidermis (Montcouquiol, 2007; Wang and Nathans, 2007).

The fly wing has been a particularly valuable system for the study of PCP due to its suitability for genetic analysis and simple tissue and cellular structure. The manifestation of planar polarity in the wing is each cell forming a single distally pointing hair. Two factors appear to control this. The *frizzled* signaling pathway functions to restrict hair initiation to the distal side of wing cells (Wong and Adler, 1993). This is thought to involve the formation of distinct protein complexes on the distal and proximal sides of wing cells (Adler et al., 2004; Axelrod, 2001; Bastock et al., 2003; Jenny et al., 2003; Strutt and Warrington, 2008; Strutt, 2001; Usui et al., 1999; Yan et al., 2008). Mutations in tissue polarity genes lead to hairs forming at alternative cellular locations (Wong and Adler, 1993). In wild type cells hairs form over a smaller part of the cell than is occupied by the distal protein complex and there is evidence that the activation of the cytoskeleton leads to a refinement or reduction in the area where hairs form (Adler, 2002). For example, multiple, shorter than normal, distally pointing hairs result from treating wing with actin antagonists such as cytochalasin D (Turner and Adler, 1998) and by mutations in genes such as *Rho kinase* or *crinkled* (myosin VII) whose wild type products normally activate the actin cytoskeleton (Kiehart et al., 2004; Turner and Adler, 1998; Winter et al., 2001).

A growing number of genes have been identified that are important for the development of *Drosophila* wing planar polarity. These include the PCP (or core) genes (*fz, disheveled* (*dsh*), *prickle/spiny leg* (*pk/sple*), *Van Gogh* (*Vang*) (aka *strabismus*), *starry night* (*stan*) (aka *flamingo*) and *diego* (*dgo*)) (Axelrod, 2001; Chae et al., 1999; Feiguin et al., 2001; Gubb et al., 1999; Usui et al., 1999; Vinson et al., 1989; Wolff and Rubin, 1998), the PPE (Planar Polarity Effector) genes (*inturned* (*in*), *fuzzy* (*fy*) and *fritz* (*frtz*)) (Collier and Gubb, 1997; Collier et al., 2005; Park et al., 1996) and the *multiple wing hairs* (*mwh*) gene (Strutt and Warrington, 2008; Yan et al., 2008). The PCP group appear to function upstream of both the PPE genes and *mwh,*

* Corresponding author.
E-mail address: pna@virginia.edu (P.N. Adler).

0012-1606/$ – see front matter © 2009 Elsevier Inc. All rights reserved.
doi:10.1016/j.ydbio.2009.06.027

and the PPE genes appear to function upstream of *mwh* (Wong and Adler, 1993). Among other genes implicated in *Drosophila* PCP is the Rho1 GTPase, which has been studied in both the eye and wing with regard to planar polarity (Strutt et al., 1997). Rho1 is particularly intriguing as a putative downstream gene as it is a well-known regulator of the actin cytoskeleton. The original observations on Rho1 in *Drosophila* wing planar polarity indicated that Rho1 mutant cells produced multiple hairs with abnormal polarity that resembled those produced by mutations in PPE genes (Strutt et al., 1997) and it was suggested that Rho1 functioned downstream of Dsh. A later paper found that mutations in the Rho effector, Rho kinase caused cells to produce multiple hairs of normal polarity (Winter et al., 2001). Hence, Rho1 would need to interact with an additional effector to alter wing hair polarity, but it remained unclear what this was. The Mwh protein recently emerged as a candidate effector (Strutt and Warrington, 2008; Yan et al., 2008).

We re-examined the phenotypes of Rho1 mutations in wing cells and found a more complex story than previously described. Clones of Rho1 mutant cells did not proliferate well, which hampered our ability to study their potential tissue polarity phenotypes. Rho1 mutant cells that survived often produced distally pointing multiple hairs that were similar to those seen in Drok mutant cells. Similar phenotypes were seen in experiments where we knocked down Rho1 levels using RNAi and when we over expressed a RhoGap expected to decrease Rho1 activity. More severe phenotypes were seen when we over expressed a dominant negative or constitutively active Rho1 protein (Van Aelst and Symons, 2002). Additional phenotypes included changes in cell shape, extreme multiple hair formation and a lack of hair formation. The cell shape changes were correlated with changes in adherens junctions as assayed by DE-cadherin immunostaining (Oda et al., 1994) and changes in septate junctions as assayed by Coracle staining (Lamb et al., 1998).

The Mwh protein was recently found to contain a GBD:FH3 domain (Strutt and Warrington, 2008; Yan et al., 2008). This motif is also found in diaphanous family formins. In that context Rho1 binding to the GBD results in the release of an autoinhibitory interaction freeing the actin binding FH1 and FH2 domains to promote actin polymerization (Goode and Eck, 2007; Rivero et al., 2005; Rose et al., 2005). Hence, Mwh is an attractive candidate for a tissue polarity protein that could mediate Rho1 function in Planar Polarity. We report here genetic experiments that argue Rho1 activates Mwh and promotes its accumulation. We also found that these two proteins could be co-immunoprecipitated from wing cells and that this interaction was mediated by the GBD:FH3 domain. Further genetic experiments established that *Rho1* also had *mwh* independent functions in wing hair development. Additionally, we found that *Rho1* mutations could alter the asymmetric accumulation of the Fz and Stan PCP proteins. The pattern of disruption was similar but not identical to that seen for DE-cadherin by alterations in *Rho1*. We suggest that the effect on PCP protein accumulation is an indirect consequence of the effects of *Rho1* on cell shape and junctions.

Materials and methods

Fly genetics

All flies were raised at 25°C. Mutant, Gal4 drivers and UAS stocks were either obtained from the *Drosophila* stock center at University of Indiana, generated in our lab or were generous gifts from J. Axelrod, D. Strutt, M. Mlodzik, T, Uemura or T. Wolff. A stock for using RNAi to knock down Rho1 expression (VDRC stock 12734) was obtained from the VDRC. The FLP/FRT technology was used to generate genetics mosaics. To direct transgene expression, we used the Gal4/UAS system. To express dominant negative or constitutively active *Rho1*, we crossed *UAS-Rho1** and *ptc-Gal4 ptub-gal80^{ts}* flies. The progeny were raised at 21°C or 18°C. White pupae were collected and grown at 25°C for 24 h and shifted to 29°C for 2–8 h before dissection, fixation and staining. For those experiments where we wanted to assess the consequences in adult flies the flies were shifted to 21°C after their incubation at 29°C. In the experiments with Rho1 effector loop mutations prepupae were collected and shifted to 29°C and left there for 24–38 h prior to dissection. Experiments that used a Rho1 dsRNA encoding transgene (line 12734 from the VDRC (Dietzl et al., 2007) used a similar long incubation at 29°C.

Immunostaining

A standard staining procedure was applied. Briefly, Fly pupae were fixed in 4% paraformaldehyde, PBS for 2 h at 4°C. After fixation, pupae were rinsed with PBS, wings were dissected and then stained with primary antibodies in PBS, 0.3% Triton X-100 and 10% goat-serum overnight at 4°C. Secondary antibodies were applied for 2–3 h at room temperature.

Plasmid constructs

mwh and Rho1 constructs subcloning for two-hybrid assays

Full-length of *mwh* cDNA was subcloned into pGADT7 vectors from NdeI–EcoRI. The following primers were used: AD-mwh5: GGAATTC-CATATGGCTCCCAGTGTGTGCG; AD-mwh3new: CCGGAATTCT-TAGTA-GAGGCCGGATGGCAG. To get the truncated form of *mwh* cDNA, we used AD-mwh5′: CCGGAATTCCATGTTTCTCAACACGTTCATTGA and the same AD-mwh3new primer. The truncated *mwh* cDNA was subcloned into pGADT7 vectors from NdeI–BamHI.

For Mwh and Rho1 interactions, the *Rho1* DGC cDNA clone GH20776 was used as the template. Full-length of *Rho1* cDNA was subcloned into pGBKT7 vector from NdeI–BamHI using the following primers: DBD-rho5′: GGAATTCCATATGACGACGATTCGCAAGAA; DBD-rho3′: CGCGGATCCTTAGAGCAAAAGGCATCTGG. The fragment encoding *mwh* GBD-FH3 was subcloned into pGADT7 vectors from Nde I–EcoRI sites. The following primers were used: MwhGBD-FH-5: GGAATTCCATATGTACAGCAAGGAAAACCAGCG; MwhGBD-FH-3: CCGGAATTCTTAGATGCCCTCGTCCTCGTG.

mwh constructs for transgenes

The cDNA coding for the GBD-FH3 domain of Mwh was amplified by PCR and subcloned into the pDORN 221 vector. Both the GBD:FH3 and Mwh-C coding regions were transferred to the pTWH gateway vector (The *Drosophila* Genomics Resource Center) to generate the desired *UAS* transgenes. Germ line transformation was by standard techniques.

Antibodies

Anti-Mwh antibodies used were described previously (Yan et al., 2008). Monoclonal anti-actin antibody and monoclonal anti-HA antibody were from Sigma-Aldrich. Monoclonal anti-phosphotyrosine antibody and polyclonal anti-GFP were from Invitrogen. Monoclonal anti-armadillo, monoclonal anti-Rho1, monoclonal anti-DE-cadherin, monoclonal anti-Coracle, monoclonal anti-Dics Large and monoclonal anti-Stan/Flamingo antibodies were obtained from Developmental Studies Hybridoma Bank (DSHB) at University of Iowa. Alexa 488- and Alexa 568-conjugated secondary antibodies were purchased from Invitrogen. Labeled phalloidin was also obtained from Molecular Probes.

Co-immunoprecipitation and western blotting

Wings discs from flies of the following genotypes were used.

w UAS-Rho1-GFP; ptc-Gal4 UAS-mwh/+
w UAS-Rho1-GFP; ptc-Gal4 UAS-mwh-C/+
w; UAS-GBD-FH3-3HA/+; UAS-Rho1-GFP/actin-Gal4.

100–150 wing discs were dissected from third instar larvae and we followed procedures described previously (He et al., 2005). Immunoprecipitations were done using either Polyclonal anti-Mwh antibody (rabbit), Polyclonal anti-HA (rabbit — Sigma/Aldrich), or polyclonal anti-GFP (rabbit — Invitrogen). Western blots were probed with either polyclonal anti-Mwh antibody (rat), monoclonal anti-HA (mouse — Sigma), monoclonal anti-Rho1 (mouse — DSHB) or monoclonal anti-GFP antibody, BD.

Results

The Rho1 mutant phenotype

Prior to carrying out genetic experiments to look for a functional interaction between *mwh* and *Rho1* we re-examined the *Rho1* mutant phenotype in wing cells. These experiments were complicated by need to balance cell and organism lethality with the desire to obtain a strong mutant phenotype. Consistent with previous reports (Strutt et al., 1997), we found that *Rho1*$^{-}$ null cells did not proliferate normally and we did not recover substantial clones. Even when we used a hypomorphic *Rho1* allele, we typically recovered only small clones. Two mutant phenotypes were seen in such clone cells. Some *Rho1* mutant cells appeared to be tetraploid (based on cell size) and these cells often formed multiple hairs, as has been seen previously in polyploid cells where the *fz* pathway was functional (Fig. 1B — arrowhead) (Adler et al., 2000). It is well established that Rho function is important in cytokinesis in *Drosophila* and other systems (Gregory et al., 2007; Hickson and O'Farrell, 2008; Narumiya and Yasuda, 2006; Prokopenko et al., 1999) so finding tetraploid cells was not surprising. In addition, some of the apparently diploid *Rho1* mutant cells produced two or three hairs of normal polarity (Fig. 1A — arrows). These resembled those produced by *Drok* mutant cells (Winter et al., 2001). Similar phenotypes were observed in experiments where we used the expression of an RNAi inducing transgene (transformant 12734 from the Vienna collection) to knock down Rho1 activity (Fig. 1D) (Dietzl et al., 2007). In such wings we also saw examples of cells that appeared not to form a hair.

In an attempt to get a stronger phenotype without cell death we directed expression of wild type, dominant negative (DN) or constitutively active (CA) Rho1 in pupae. The directed expression of a wild type Rho1 protein had little consequence. This is presumably due to Rho1 activity being regulated post-translationally. The directed expression of the DN or CA proteins for an extended period of time was lethal. Hence we used a temperature sensitive GAL80 protein (McGuire et al., 2003) and temperature shifts to limit the expression of the Rho1 protein to a short period of time (2–8 h). In these experiments we usually used *ptc-Gal4* to drive expression and often examined pupal wings as this enabled us to observe more severe phenotypes in animals that would not eclose (animals kept for more than 4 h at 29°C rarely eclosed). The expression of DN-Rho1 (Rho1-N19) led to a phenotype that overlapped with loss of function mutant clones (Figs. 1C, E). In pupal wings we observed cells that did not form a hair (Fig. 2N — asterisks), cells that appeared delayed in hair formation, polyploid cells and occasional multiple hair cells that appeared to be diploid (Figs. 2M, N — arrows). The vast majority of hairs formed at the distal most vertex/side of cells but some appeared to form at an alternative location and to not point distally. Most of these were oriented about 60° from distal (Figs. 2M, N — arrows). Wing regions where DN-Rho1 was expressed were thinner than neighboring regions with increased cell width and decreased cell height (Figs. 2E–I — asterisks, 3A — #). These cells also had lower F-actin staining (Supplementary Fig. 1). In extreme cases many cells in the *ptc* domain were lost leading to a wing with a hole (Supplemental Fig. 2). We often saw abnormalities in tissue structure after expression of DN-Rho. These included cells that appeared to be located between the two cell layers, places where the epithelium appeared to be two cells thick and places where cells appeared to be in the process of leaving the epithelium from the apical surface (Fig. 2H — arrowhead).

The dramatic changes in the shape of pupal wing cells were unexpected. Since these experiments involved the over expression of a dominant negative protein we were concerned that they might due to a loss of specificity and not reflect the normal function of *Rho1*. To assess this we enhanced the knockdown obtained using a *Rho1* RNAi inducing transgene (stock 12734 from VDRC) by simultaneously including a *UAS-dicer2* transgene (Dietzl et al., 2007). We examined *ptc-Gal4 Gal80*^{ts}*/UAS-Rho1-dsRNA; UAS-dicer2/+* pupal wings that had been at 29°C for 26–36 h and as was the case for the directed expression of DN-Rho1, we observed cells that had decreased height, increased cross sectional area and decreased F-actin (Figs. 2O, P, 3F). The phenotypes in the enhanced knock down wings were not quite as severe as the strongest seen with the expression of DN-Rho1. Wings resulting from the two treatments differed as in the knock down the dorsal and ventral layers separated basally leaving an internal hole (Figs. 2O, P — asterisks). The basis for this difference was unclear but might be due to the kinetic differences (i.e. a much longer period of induction was required for the RNAi knock down to get a strong phenotype). In both types of experiments the extent of cell shape change was variable across the *ptc* domain, resulting in "wavy" wings comprised of cells of varying heights (Supplemental Fig. 3). That we saw similar cell shape changes by these two different approaches confirmed that the phenotype was not due to a loss of specificity with over expression.

We found that the expression of CA-Rho1 (Rho1-V14) led to cells bulging apically, forming multiple hairs of relatively normal polarity (arrows), and showing increased cortical F-actin staining (arrowheads) (with decreased cytoplasmic actin staining) (Figs. 1H, I, 2A–D, J–L). The multiple hair cell phenotype could be quite severe with cells forming 10 or more short hairs that pointed upward from the wing surface (Figs. 1H, I — arrows). We suspect that this abnormal vertical orientation is due to a defect in one or more late steps in hair morphogenesis. Some cells almost had a "ridge of hair formation"

Fig. 1. The adult wing phenotype of *Rho1* mutations. Panels show bright field micrographs of adult wings with phenotypes that result from *Rho1* mutations or mutations in associated factors. Unmarked *Rho1* mutant clones (A–B) can be identified by the Rho1 mutant phenotype. The arrowhead points to a likely polyploid cell (Polyploid cells can be identified due to increased spacing between the hair it produces and its neighbors. They can also be identified due to forming a longer hair when they form a single hair and to longer than expected hairs when they form multiple hairs (regardless of ploidy when a cell forms multiple hairs they are smaller than an equivalent cell that formed a single hair) (Adler et al., 2000) and the arrows to presumptive diploid cells that formed two hairs of normal polarity. The clone in A is the largest *Rho1* clone we have seen. A more typical smaller *Rho1* clone (B) is also shown. The arrowhead (B) points to a likely polyploidy cell that formed multiple hairs. Note the polarity of the hairs is relatively normal. The dorsal surface (C) and ventral surface (E) of *ptc-GAL4 tub-GAL80*^{ts}*/+; UAS-Rho1 N19/+* wings from flies kept at 29°C for less than 4 h. These represent the typical range of phenotypes seen in this genotype treated in this way. The arrowheads point to multiple hair cells that appear to be polyploid. The arrows point to apparently diploid cells that formed two hairs. Note that these cells have normal polarity. The asterisk is located over an area where cells did not appear to form a hair. Wings from *ptc-GAL4 tub-Gal80*^{ts} *UAS-Rho1-dsRNA/+* flies produce multiple hair cells (D) (arrows). Wings from *ptc-GAL4/+; UAS-RhoGAP P190/+* wings from flies grown at 21°C (F) or 29°C (G) contain multiple hairs of normal polarity (arrows). Note that the phenotype is stronger at 29°C. This is due to the Gal4 being more active at 29°C than 21°C. Wings from *ptc-GAL4 tub-Gal80*^{ts}*/UAS-Rho1 v14* flies (HI). The arrows (HI) point to cells that show the extreme multiple hair cell phenotype induced by CA-Rho1. The arrowheads (H) point to bulged cells with their "domed" phenotype. Such cells will usually form hairs but they are out of the plane of focus in this image. A wing with a flip out clone (see arrow) where *actin-GAL4* drives expression of *UAS-Rho1 v14* (J). Note the two cells with an extreme multiple hair cell phenotype and a bulged cell surface (arrowhead). A wing from a region of a *ptc-GAL4 tub-Gal80*^{ts}*/UAS-Rho1 v14; mwh*^{1} wing (K). These animals rarely eclosed so their wings were not pumped out and flat. The arrow points to a *mwh* cell that was not affected by Rho1 v14. The asterisk is on a bulged cell within the *ptc* domain. These cells also express an extreme multiple hair cell phenotype (arrowhead). Wings from *mwh*^{1} (L) wing and *ap-Gal4/UAS-GFP-Rho1; mwh*^{1} (M) flies from the same experiment are shown for comparison. Both images show the same wing region. Wings from *mwh*^{6}*/mwh*^{1} (N) and *ptc-Gal4/UAS-RhoGAP-P190; mwh*^{6}*/mwh*^{1} (O) flies from the same experiment (animals raised at 21°C).

(Figs. 2J, K — arrow). The multiple hair phenotype is reminiscent of that of *tricornered* or *furry* mutant cells, although more severe (Cong et al., 2001; Geng et al., 2000). Most of these cells formed hairs on the distal side but some showed hair formation at an alternative face/vertex, most often about 60° from distal (see Figs. 2J, K). The increased cortical F-actin and the apical bulging could be seen clearly in *Z* sections, which also showed that the cells were often shorter than normal. A number of cell shape phenotypes were detected that appeared to represent different degrees of severity (Figs. 2A–D — arrows). Weakly affected cells appeared rounder but did not obviously disrupt the normal flat apical surface of the tissue. More severely affected cells were rounded and not flat apically. Still more severely affected wings showed examples where a cell no longer appeared to be attached at the normal basal surface leading to an epithelium that appeared to be two cells thick in places (Fig. 2C). Such wings often contained cells that appeared to be in the process of being expelled from the epithelium (Fig. 2D — arrow).

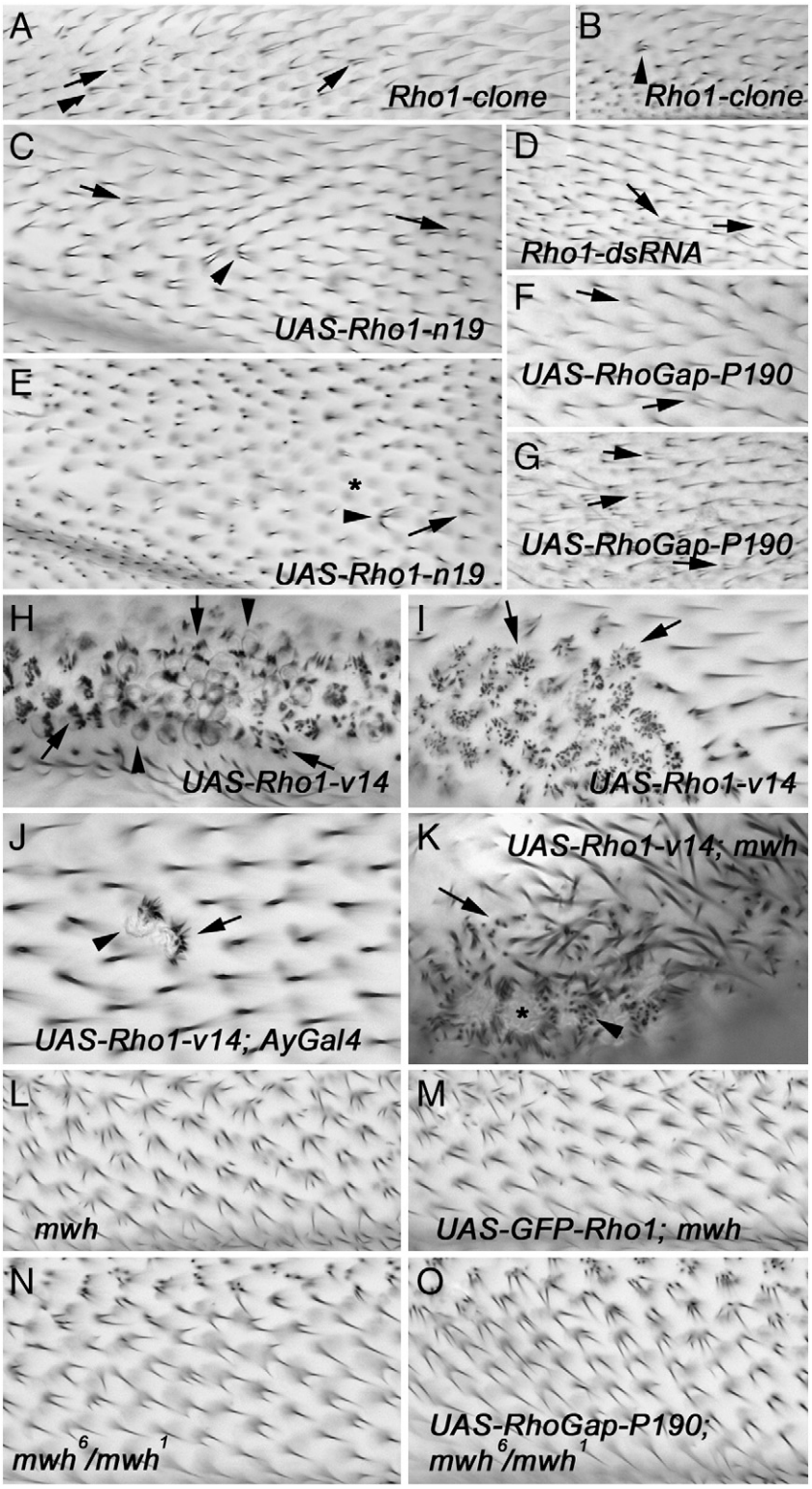

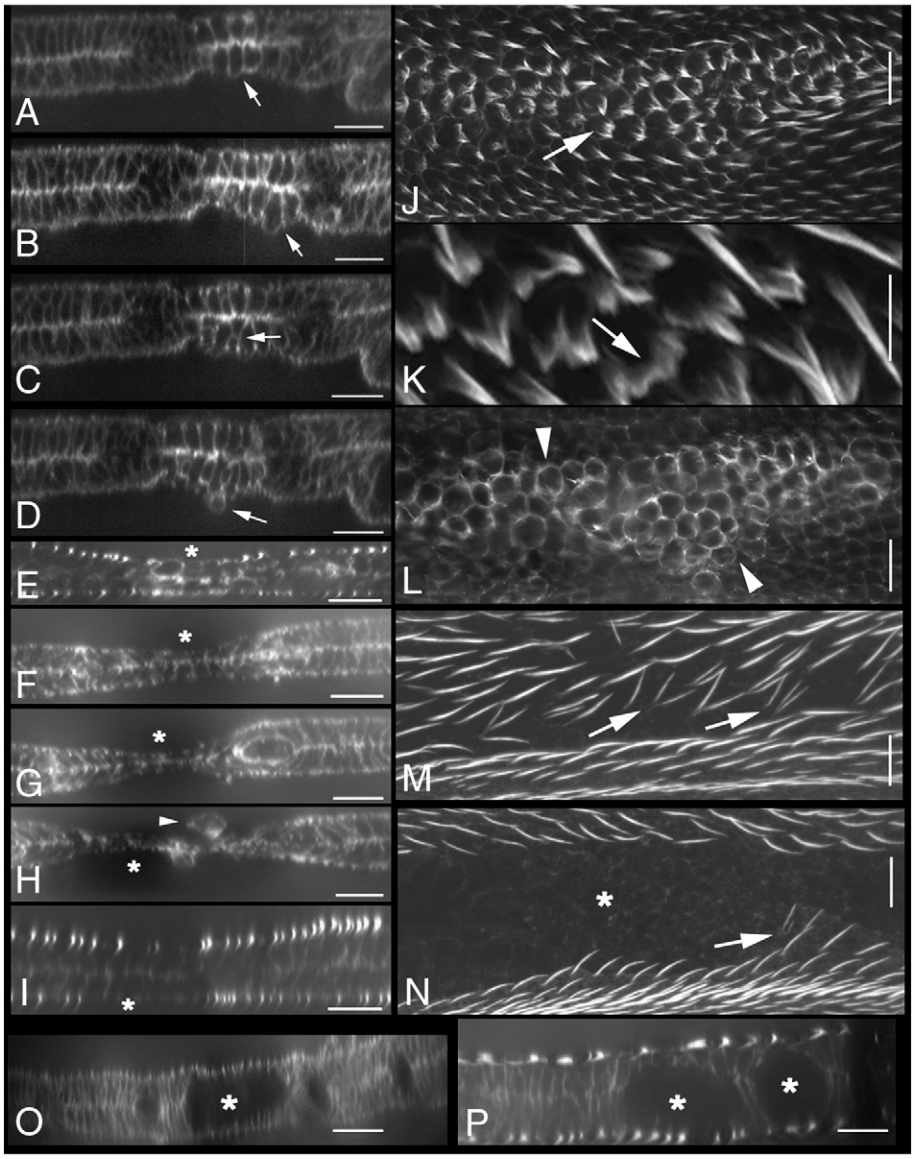

Fig. 2. The affects of DN and CA-Rho1 on pupal wings. *Z* axis reconstructions of *ptc-GAL4 tub-Gal80^{ts}/UAS-Rho V14* pupal wings kept for from 4 to 8 h at 29°C (A–D). The wings were stained for F-actin. The strength of the phenotype increases as one goes from A to D. Arrows points to the middle of the *ptc* domain (A). Cells in this region show increased cortical and basal F-actin staining and a rounded shape. Successively stronger phenotypes (B–D) are shown. Note the cells are apically bulged (B) (arrow). There is an example of where there appears to be one cell on top of another (C) (arrow) and one where a cell appears to be in the process of being expelled apically from the epithelium (D) (arrow). *Z* axis reconstructions of *ptc-GAL4 tub-Gal80^{ts}/+; UAS-Rho N19/+* wings kept for 4–8 h at 29°C (E–I). Progressively stronger phenotypes can be seen. The asterisks mark the center of the *ptc* domain. Note how the cells in this region become progressively shorter and there is a decrease in general F-actin staining. Although not obvious in this set of images they also appear to have increased cross section. In one image (H) two cells (arrowhead) are either being expelled from the epithelium or blood cells are attaching to the epithelium at this location. In another (I) hair formation has been blocked in many of the cells in the *ptc* domain. It is a *Z* axis reconstruction from the same wing shown in N. The hairs appear as bright spots of F-actin at the apical surface of the cells (arrow). A planar view of a *ptc-GAL4 tub-Gal80^{ts}/UAS-Rho V14* wing kept for from 6 h at 29°C (J). The wing is 34 h apf (after white prepupae formation) and hair growth is under way. The image is centered over the *ptc* domain and the extreme multiple hair cell phenotype is seen (arrow). A blow up of part of this image (K) allows additional details to be seen. Note the most extreme cells (arrow) show almost a ridge as opposed to a hair growing. A dramatic phenotype can also be seen in a *ptc-GAL4 tub-Gal80^{ts}/UAS-Rho V14* pupal wing kept at 29°C for 6 h (L). This wing is 31 h apf and hairs have not started forming. The rounded shape and enhanced cortical F-actin staining is obvious (arrowheads). Planar views of the dorsal (M) and ventral (N) surfaces of *ptc-GAL4 tub-Gal80^{ts}/+; UAS-Rho N19/+* wings kept for 6 h at 29°C show multiple hair cells (arrows). Hair polarity is only slightly abnormal in most cases. For example, are the hairs pointing about 60° from distal (N) (arrow). An asterisk is located over a large region where hair formation did not take place (N). *Z* axis reconstructions of *ptc-Gal4tub-Gal80^{ts}/+; UAS-Rho-dsRNA/UAS-dicer2* pupal wings from pupae grown at 21°C, shifted to 29°C at wpp and kept there for 26–28 h prior to dissection (OP). Note the regions marked by asterisks where the dorsal and ventral cells are shorter than their non-*ptc* domain neighbors and no longer attached basally. In all images except K the scale bar is 10 μm. For K it is 5 μm.

The ability of CA-Rho1 to induce mutant phenotypes requires that the mutant protein transduce its active state to downstream components. This is accomplished by the interaction of downstream proteins with part of the Rho protein — the effector loop. In mammalian cell culture experiments effector loop mutations have been identified that show specificity in blocking particular downstream effectors (Sahai et al., 1998; Zohar et al., 1998). For example, the ability of CA-Rho to stimulate stress fiber formation in NIH3T3 cells was blocked when the F39V mutation was simultaneously present but the ability to activate transcription by Serum Response Factor was not blocked. In contrast, both outputs were blocked in E40L mutants. Mlodzik et al. (Fanto et al., 2000) placed the analogous effector loop mutations into *Drosophila* CA-Rho1 transgenes and found that the differential effects of the F39V and E40L mutations was conserved in the eye. When expressed in the pupal wings both effector loop mutations severely suppressed the cell shape alterations and multiple hair cell phenotypes seen with CA-Rho1 (data not shown). With long-term expression (24–36 h) of the transgenes we saw a weak hair

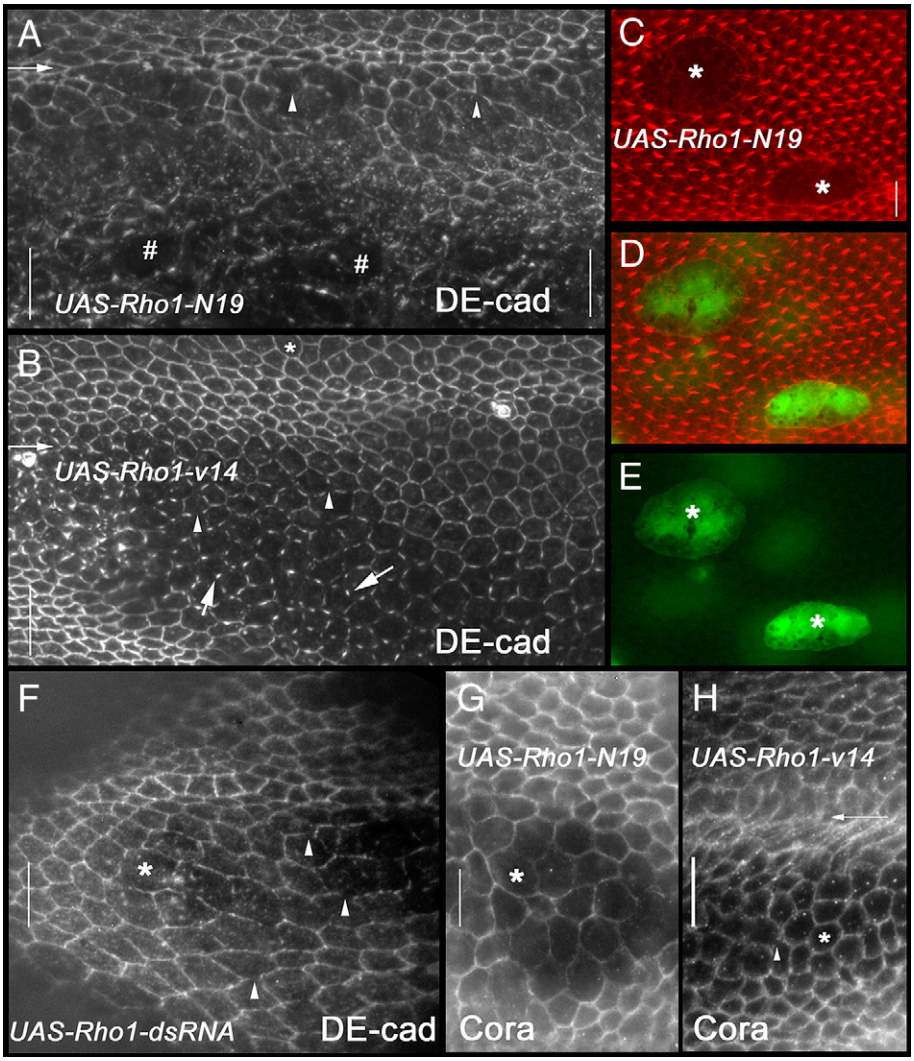

Fig. 3. Mutant Rho proteins can influence DE-cadherin accumulation and cell adhesion. A *ptc-GAL4 tub-Gal80^{ts}/+; UAS-Rho N19/+* wing from a larva kept for 6 h at 29°C and immunostained for DE-cadherin (A) shows gaps in cadherin staining (arrowheads). The arrow points to the edge of the *ptc* domain. The #s are located over cells with unusually large cross section and with only small regions of DE-cadherin staining. A *ptc-GAL4 tub-Gal80^{ts}/UAS-Rho V14* wing kept at 29°C for 6 h was stained for DE-cadherin (B). The small arrow points to the edge of the *ptc* domain. The bright staining cells with smaller cross section just above this are wing vein cells. The arrowheads points to gaps in cadherin staining that are centered over tri-cellular junctions. The large arrows point to patches of bright DE-cadherin staining and the * to regions outside of the *ptc* domain with normal levels of DE-cadherin. Flip-out clones marked by the expression of GFP (green) (asterisks) that also over express DN-Rho1 (*w hs-flp; AyGal4 UAS-mcd8-GFP/+; UAS-Rho1-N19/+*) (C–E). F-actin staining is shown in red. Note the low level of F-actin staining in the clone cells and the smooth borders of the clone cells. A pupal wing from a *ptc-Gal4tub-Gal80^{ts}/+; UAS-Rho-dsRNA/UAS-dicer2* animal grown at 21°C, shifted to 29°C at wpp and kept there for 26–28 h prior to dissection is shown (F). The tissue was stained for DE-cadherin. The asterisks over a cell with a larger than normal cross sectional area and the arrowheads point to locations where the lattice of DE-cadherin staining is interrupted. A *ptc-GAL4 tub-Gal80^{ts}/+; UAS-Rho N19/+* wing from a pupa kept for 6 h at 29°C was immunostained for Coracle (Cora), a SJ marker (G). The asterisks is over a cell with a larger than normal cross section. Overall Cora levels are lower in the most affected cells but there are only small regions where the lattice is interrupted. A *ptc-GAL4 tub-Gal80^{ts}/UAS-Rho V14* wing from a pupa kept at 29°C for 6 h (H). The wing was stained for Cora. The small arrow points to the vein at the edge of the *ptc* domain, where the tissue bulges. The asterisk is located over a rounded cell and the arrowhead points to a region where there is a gap in the lattice of Cora staining. All of the scale bars are 10 μm.

morphology phenotype (primarily thickened hairs) with incomplete penetrance that in its strongest form was equivalent to what we saw with 2–4 h of expression of RhoV14. We concluded that the cell shape and hair phenotypes were a consequence of Rho1 activity being transduced in the cytoplasm to the cytoskeleton (i.e. equivalent to the mechanism used in mammalian cells to induce stress fibers).

An alternative way we used to get around the cell lethality of *Rho1* mutations was to induce Gal4 flip-out clones (Struhl and Basler, 1993; Buenzow and Holmgren, 1995) in prepupae to drive expression of either constitutively active or dominant negative Rho1 proteins in a limited set of cells for a limited time. This approach gave results that were similar to those obtained using the *gal80-ts* approach (Fig. 1J). We also examined pupal wings that contained marked flip out clones that expressed a DN-Rho1 (Figs. 3C–E). The increased cross section and decreased F-actin in such cells was reminiscent of the phenotypes seen using the *gal80-ts* approach. An interesting observation was that the clones were rounded without the interdigitating borders usually seen with clones in pupal wings. This suggested that the expression of DN-Rho1 altered cell–cell adhesion.

We also examined the consequences for wing hair morphogenesis of modulating the activity of Rho1 regulators and effectors. A notable result was that the over expression of RhoGap P190, which should lead to decreased Rho activity (Billuart et al., 2001) led to the formation of occasional multiple hair cells (Figs. 1F, G — arrows). This was not seen when a mutant RhoGap P190 (R1389L) was expressed implying that it was the Rho regulatory activity of Rho Gap P190 that was the cause of the multiple hair cells (Ng and Luo, 2004).

Rho1 regulates DE-cadherin accumulation in pupal wing cells

The dramatic cell shape changes and apparent changes in cell–cell adhesion associated with altered Rho1 function suggested that proteins

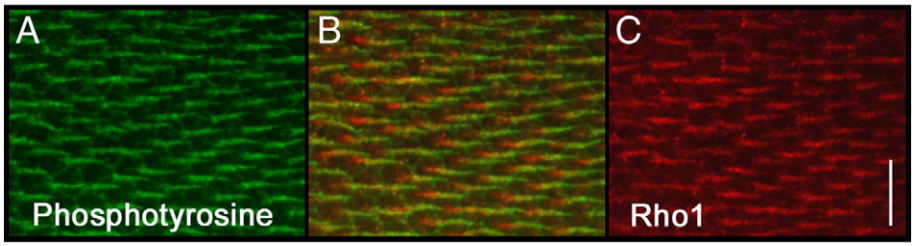

Fig. 4. Rho immunostaining in pupal wing. A pupal wing stained with both anti-Phosphotyrosine (green) (A) and anti-Rho1 (red) (C) antibodies. A merged image is also provided (B). Note the accumulation of Rho1 in growing hairs. The phosphotyrosine staining of the hair is restricted to the region near the cell surface while the Rho1 staining extends below the cell surface as part of the hair "root". The scale bar is 10 μm.

involved in the maintenance of epithelial cell structure and adherens junctions might also be affected. Cadherins are central to the formation of adherens junctions (AJ) and are prominent markers for them (Gumbiner, 2005). We immunostained pupal wings that expressed DN-Rho1 and found that this resulted in a dramatic down regulation of DE-cadherin (Fig. 3A). In some cells no cadherin staining remained while in others small patches of staining remained that presumably represented regions where the AJ remained intact. In the least affected cells gaps were seen in cadherin staining (Fig. 3A, arrowheads). We also immunostained wings that had the enhanced knock down phenotype. The most strongly affected cells showed prominent gaps in DE-cadherin staining (Fig. 3F) that once again appeared to be a weaker version of what we saw with the directed expression of DN-Rho1.

In cells that expressed a CA-Rho1, DE-cadherin staining was interrupted although not as severely as when the DN-Rho1 was expressed (Fig. 3B). Interestingly, the staining gaps were often centered on tri-cellular junctions (arrowheads). In moderately affected regions many of the small regions of staining that remained appeared brighter (Fig. 3B large arrows) than the staining of non-vein cells outside of the *ptc* domain (Fig. 3B asterisk). We quantified this using Image J and found that the difference was significant (ratio inside *ptc* domain/outside = 1.49, $n = 40$, *t*-test $p = 1 \times 10^{-11}$). Thus, CA-Rho1 expression resulted in a reorganization of DE-cadherin that included both local increases and decreases.

In *Drosophila* epithelial cells the septate junction (SJ) is located just basally to the adherens junction and both sets of junctions are part of the normal machinery of apical/basal polarity. To determine if alterations in Rho1 also affected SJs we immunostained pupal wings expressing either DN or CA-Rho1 for the SJ component Coracle (Lamb et al., 1998). The increased cell cross section seen with the expression of DN-Rho1 was obvious after anti-Cora immunostaining (Fig. 3G) but the continuity of the SJ did not appear to be as profoundly altered as the AJ did. Some gaps were seen in the SJ after the directed expression of CA-Rho1 (Fig. 3H) but once again the effects were much less prominent than we saw for DE-cadherin staining. In an independent set of experiments we used anti-Discs Large (Woods and Bryant, 1991) immunostaining to visualize the SJ and obtained similar results (data not shown).

Rho1 in the pupal wing

Asymmetric protein accumulation in pupal wing cells is a characteristic shared by members of the *fz* pathway (Adler et al., 2004; Axelrod, 2001; Jenny et al., 2003; Shimada et al., 2001; Strutt and Warrington, 2008; Strutt, 2001; Tree et al., 2002; Usui et al., 1999; Yan et al., 2008). We immunostained pupal wing cells prior to hair formation with anti-Rho antibody and found Rho1 widely distributed in wing cell cytoplasm with a slight peripheral preference, but there was no evidence of preferential localization to either the proximal or distal edges (Supplementary Fig. 1). Once hair morphogenesis started, Rho1 accumulated in growing hairs (Fig. 4). This was not surprising as in many cell types Rho1 both regulates and localizes with the actin cytoskeleton and the hair is rich in F-actin

Table 1
Genetic interactions between *mwh* and *Rho1*.

Line	Genotype	Temp[a]	Mean hairs/cell	SE	Different $p<0.001$	Different $p<0.05$	Number of cells scored
1	*mwh*^{1}	25 °C	3.62	0.045	NR	NR	609
2	*Rho1/+; mwh*^{1}	25 °C	3.52	0.042	1[b] — no	1 — no	604
3	*ap-GAL4;mwh*^{1}	25 °C	3.49	0.042	1 — no	1 — no	602
4	*ap-GAL4/UAS-GFP Rho; mwh*^{1}	25 °C	2.52	0.035	1, 3 — yes		607
6	*mwh*^{6}	25 °C	1.56	0.026	1 — yes		501
7	*mwh*^{6}	21 °C	1.25	0.019	6 — yes		600
8	*mwh*^{1}/*mwh*^{6}	21 °C	1.83	0.030	7 — yes		600
9	*Rho1/+; mwh*^{1}/*mwh*^{6}	21 °C	2.00	0.030	8 — yes		600
10	*ptc-GAL4/+; mwh*^{1}/*mwh*^{6}	21 °C	1.81	0.029	8 — no	8 — no	601
11	*ptc-GAL4/UAS-Rho GAP P190; mwh*^{1}/*mwh*^{6}	21 °C	2.13	0.034	8 — yes 10 — yes		659
12	*ptc-GAL4/UAS-Rok-CAT; mwh*^{1}/*mwh*^{6}	21 °C	1.62	0.027	8 — yes 10 — yes		600
13	*ptc-GAL4/UAS-Rok-CAT-KG; mwh*^{1}/*mwh*^{6}	21 °C	1.78	0.030	8 — no 10 — no 12 — yes	8 — no 10 — no	601
14	*ap-GAL4/+; mwh*^{1}/*mwh*^{6}	21 °C	1.87	0.031	8 — no	8 — no	600
15	*ap-GAL4/UAS-GFP-Rho; mwh*^{1}/*mwh*^{6}	21 °C	1.74	0.030	8, 14 — no	8, 14 — yes	601
16	*mwh*^{1}/*mwh*^{6}	25 °C	2.52	0.032	8 — yes		600
17	*ptc-GAL4/+; mwh*^{1}/*mwh*^{6}	25 °C	2.54	0.033	16 — no	16 — no	601
18	*ptc-GAL4/UAS-Rho-GEF2; mwh1/mwh*^{6}	25 °C	2.18	0.032	16, 17 — yes		592
19	*ptc-GAL4 Gal-80-ts/+; mwh*^{1}/*mwh*^{6}	25 °C	2.47	0.032	16 — no	16 — no	602
20	*ptc-GAL4 Gal-80-ts/UAS-Rho-v14; mwh*^{1}/*mwh*^{6}	25 °C	2.22	0.029	16, 19 — yes		597

[a] Indicates the temperature the pupae were kept at during pupal development.
[b] The number refers to the row in the table of the genotype that is being compared with the genotype of the indicated row. For example, in row 2, 1[b] indicates that the average number of hairs for genotype 2 is compared to genotype 1.

(Wong and Adler, 1993). As a control that the Rho1 monoclonal antibody staining was specific in this tissue we immunostained pupal wings where an RNAi transgene was expressed to knock down Rho1 in the *ptc* domain (Dietzl et al., 2007). A clear and dramatic decrease in Rho1 staining was seen confirming the specificity of the antibody in this tissue (Supplementary Fig. 1).

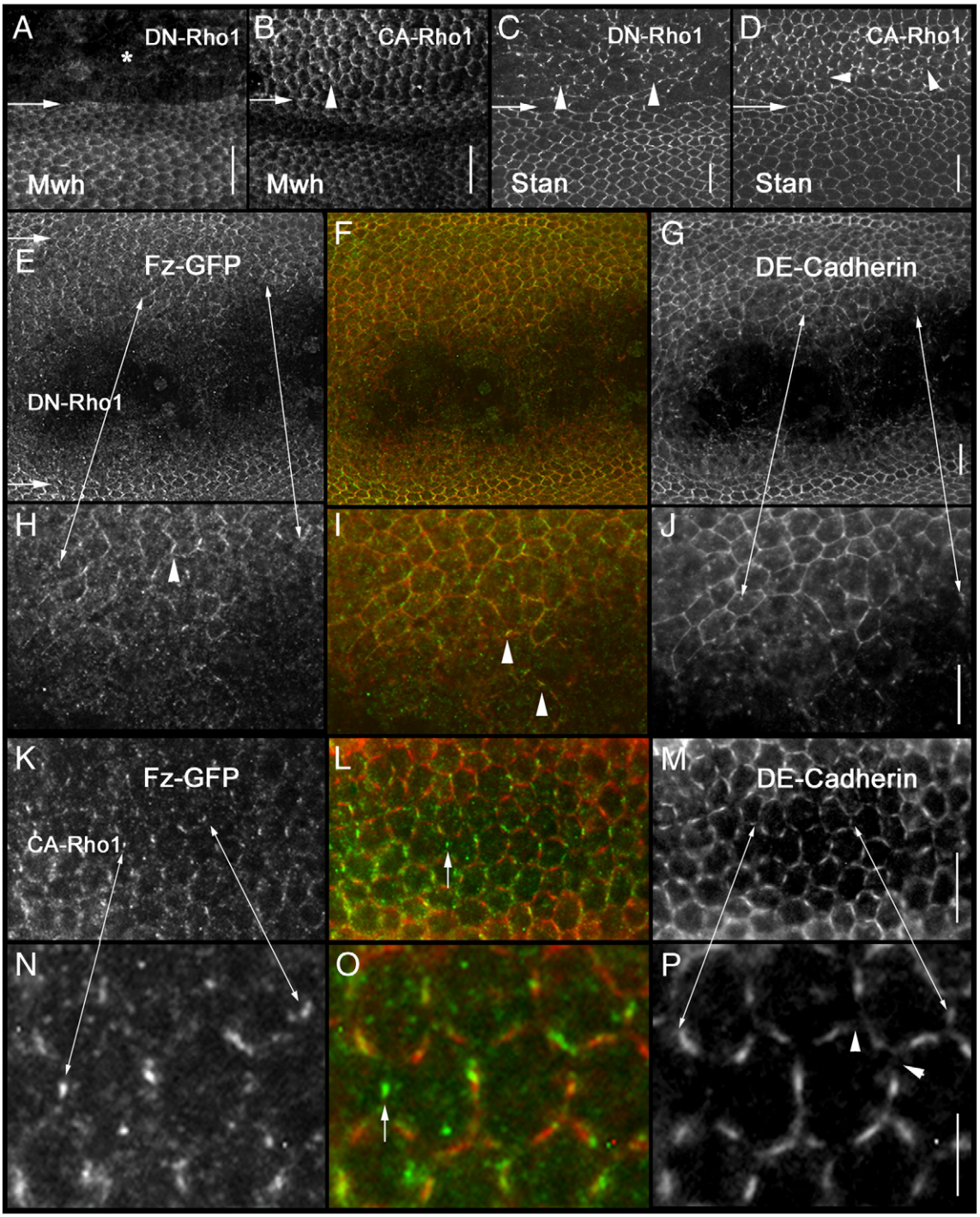

Fig. 5. Rho mutations alter the accumulation of PCP proteins. Wings from a *ptc-GAL4 tub-Gal80^{ts}/+; UAS-Rho N19/+* (dominant negative) pupae (AC) and ptc-*GAL4 tub-Gal80^{ts}/UAS-Rho V14* (constitutively active) pupae (BD) are shown. In each of these cases the horizontal arrow marks the boundary of the *ptc* domain. In all four cases the wings kept at 29°C for 6 h to induce the transgene. Wings stained with anti-Mwh antibody (AB) show the loss of Mwh staining when DN-Rho1 is expressed (A) (asterisks) and increased Mwh when CA-Rho1 is expressed (B) (arrowhead). Wings stained with anti-Stan antibody show gaps in Stan staining (arrowheads) when DN-Rho1 is expressed (C). The gaps are similar to those seen previously for DE-cadherin. Increased Stan staining was seen in cells that expressed the CA-Rho1 (D). A *ptc-GAL4 tub-Gal80^{ts}/+; UAS-Rho N19* (dominant negative)/*arm-fz-GFP* wing from a pupa kept at 29°C for 6 h to induce the transgene is shown at 2 different magnifications (E–J). The wing was stained with anti-DE-cadherin (red) and anti-GFP (green). The single color images are shown in grayscale to maximize contrast. The horizontal arrows mark the boundaries of the *ptc* domain. Note the decrease in both DE-cadherin and Fz in the *ptc* domain. The typical zig zag accumulation pattern of Fz can be seen outside of the *ptc* domain. This is lost inside the domain. The small double headed arrows point to landmarks in the two sets of images. The arrowhead (H) points to a cell that shows the typical zigzag Fz accumulation pattern. In the merged image (I) arrowheads point to highly abnormal regions that show a cell with a patch that brightly stains for both DE-cadherin and Fz. A *ptc-GAL4 tub-Gal80^{ts}/+; UAS-Rho V14/arm-fz-GFP* wing from a pupa kept at 29°C for 6 h to induce the transgene is shown at two different magnifications (K–P). The arrows (LO) point to a place in a cell where Fz-GFP is present while DE-cadherin is missing. The small double headed arrows point to landmarks in the two sets of images.

Genetic interactions between Rho1 and Mwh

Previous experiments found that *fz* pathway function was sensitive to *Rho1* gene dose (Strutt et al., 1997) and that hair number in PCP mutants was sensitive to *mwh* dose (Wong and Adler, 1993). Hence, we tested the ability of a reduction in *Rho1* gene dosage to enhance/suppress both null and hypomorphic *mwh* alleles. For the hypomorphic genotype we primarily used mwh^6/mwh^1 heteroallelic heterozygotes. The mwh^6 is a hypomorphic temperature sensitive allele (Yan et al., 2008) (see Table 1, lines 6, 7, 8, and 16) and we found it useful to carryout experiments at several temperatures. The mwh^1 allele is a null allele (Strutt and Warrington, 2008) and the heteroallelic heterozygotes have an intermediate phenotype (e.g. Table 1, lines 1, 6 and 16).

We found that over expression of wild type Rho1 protein could weakly suppress the hypomorphic phenotype seen in mwh^6/mwh^1 (Table 1, line 8 and 14 vs 15) flies. The low level expression of a CA Rho1 also partially suppressed the phenotype of mwh^6/mwh^1 (Table 1, line 16 and 19 vs 20), as did the expression of *Rho-Gef2* (Table 1, line 16 and 17 vs 18). Similarly we found that a reduction in *Rho1* dose acted as a dominant enhancer of mwh^6/mwh^1 (Table 1, line 8 and 9). The directed expression of *RhoGap P190* similarly enhanced the mwh^6/mwh^1 phenotype (Table 1, line 8 and 10 vs 11, Figs. 1N, O). These observations were consistent with Mwh being activated by Rho1 and were consistent with the dose relationships seen in the eye between *Rho1* and planar polarity genes (Strutt et al., 1997). To determine if the ability of Rho1 to modulate the phenotype of mwh^6/mwh^1 flies might be mediated by Rho kinase we expressed the catalytic domain of Rho kinase using *ptc-Gal4.* The expression of this constitutively active protein fragment partly suppressed the mwh^6/mwh^1 phenotype (Table 1, line 8 and 10 vs 12)). This was not seen with a kinase dead mutant protein (Table 1, line 8 and 10 vs 13). Thus, the ability of Rho1 to modulate the mwh^6/mwh^1 phenotype is likely mediated, at least in part, by the activation of Rho kinase.

The dosage relationship seen between mwh^6/mwh^1 and *Rho1* was consistent with the hypothesis that Rho1 activated Mwh but it did not rule out other mechanisms such as the proteins acting in parallel. To determine if Rho1 acted in parallel to Mwh we asked if altering Rho1 activity could affect hair morphogenesis in a cell that lacked any Mwh activity. We found that over-expressing Rho1 protein could partly but significantly suppress a null *mwh* phenotype (Table 1, line 1 and 3 vs 4, Figs. 1L, M). This demonstrated that Rho1 could influence hair morphogenesis in a *mwh* independent way and that at least part of *Rho1*'s effect on hair morphogenesis was mediated in parallel to *mwh*. Independent confirmation of this came in an experiment where we found that the expression of CA-Rho1 in a mwh^1 null mutant background resulted in an extreme multiple hair cell phenotype that was far more severe than that seen in mwh^1 wings (Fig. 1K). Hence this phenotype was also at least partly independent of *mwh*.

Rho1 regulated Mwh accumulation

Mwh is the only member of the *fz* pathway known to accumulate in growing hairs (Yan et al., 2008). Mwh contains a GBD-FH3 domain, a motif that is also found in diaphanous family formins where it mediates the binding of Rho1 and activation of the formin. Hence, we hypothesized that Rho1 function in wing PCP was mediated by binding to and activating Mwh. Our observation that Rho1 accumulated in the hair but not specifically on the proximal side of pupal wing cells suggested that Rho1 contributed to late *mwh* function, but did not rule out an early function in planar polarity as well.

If Rho1 regulated Mwh activity, it might do so by altering the subcellular localization or accumulation of Mwh. To test this we immunostained Mwh in cells that expressed either a DN or CA-Rho1. (These approaches gave the strongest and most reproducible *Rho1* hair phenotypes.) The accumulation of Mwh dramatically decreased in cells that expressed DN-Rho1 (Fig. 5A — asterisks), and increased in cells that expressed CA-Rho1 (Fig. 5B — arrowhead). The polarized accumulation of Mwh in cells that expressed CA-Rho1 appeared to be enhanced. This could be evidence of active Rho1 promoting the proximal accumulation of Mwh but it might also be an indirect effect of CA-Rho1 on cell shape. These observations established that Rho1 acted upstream of and positively regulated Mwh accumulation. The experiments described earlier with the effector loop mutations suggested this was mediated at a post-transcriptional level.

Does Rho1 bind to the Mwh GBD?

We found that Rho1 and full length Mwh could be co-immunoprecipitated (co-IP) from wing disc cells consistent with these two proteins functioning together in wing PCP (Fig. 6A). In these experiments only a small fraction of the total cellular Rho1 was pulled down by anti-Mwh antibody (1%–0.5%), but it was a consistent result. We suspect this is due to Rho1 being present in substantially higher amounts than Mwh in the wing disc cells used in these experiments, although other explanations such as the interaction being only weakly stable under our IP conditions are possible. Our hypothesis was that the co-immunoprecipitation was mediated by the binding of Rho1 to the Mwh GBD:FH3 domain. As a first test of this hypothesis we obtained transgenic animals that expressed Mwh fragments using UAS-Gal4. The first transgene expressed the C-terminal part of the protein that is encoded by the large 3′ most exon

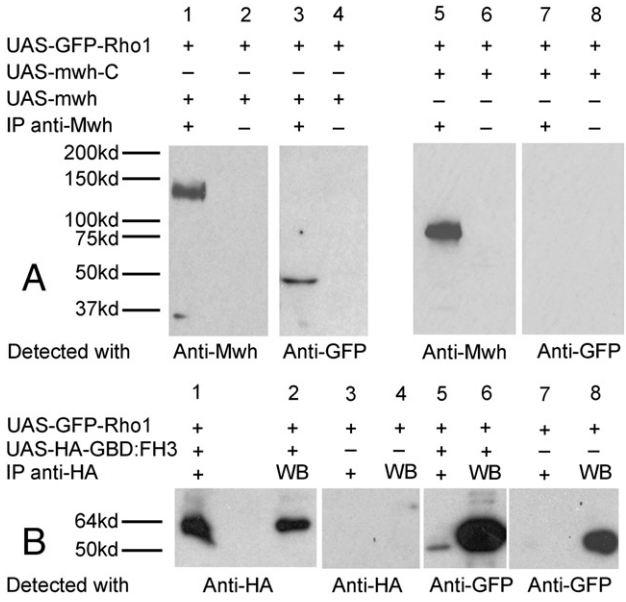

Fig. 6. Co-immunoprecipitation of Mwh and Rho1. Panel A is from an experiment where we detected the co-immunoprecipitation of Mwh and GFP-Rho but not that of Mwh-C and GFP-Rho. In these experiments expression of the transgenes in third instar wing discs was driven by *ptc-Gal4.* Extracts were treated with polyclonal rabbit anti-Mwh antibodies or not (as a control). When both UAS-Mwh and UAS-GFP-Rho1 were expressed both were detected after precipitation with anti-Mwh antibody but not in control tubes that did not contain antibody. In contrast equivalent treatment of samples from wing discs expressing UAS-Mwh-C and UAS-GFP-Rho lead to the detection of Mwh-C but not GFP-Rho1. This experiment shows that a region of Mwh deleted in Mwh-C was required for the interaction between Mwh and Rho. This experiment also serves as a control to show that the anti-Mwh antibody does not recognize and pull down GFP-Rho by itself (i.e. Mwh is needed). Several additional controls are shown in Supplementary Fig. 4. Panel B shows that the Mwh GBD:FH3 domain fragment also co-immunoprecipitates with GFP-Rho1. Western blot analysis of extracts made from wing discs that expressed UAS-HA-GBD:FH3 contained a band of the expected size that was recognized by anti-HA antibody. This band was not seen when the transgene was not present demonstrating the specificity of the blot. Equivalent control western blots are shown for GFP-Rho1 and anti-GFP antibody. When both HA-GBD:FH3 and GFP-Rho1 were expressed both were detected after precipitation with anti-HA antibody but GFP-Rho1 was not detected in the anti-HA precipitate if HA-GBD:FH3 was not expressed.

(aa 335–836). This fragment lacks the GBD (aa 60–275) but contained part of the FH3 domain (aa 290–492). The second fragment contained only the GBD:FH3 domain (Fig. 6) (aa 61–492). Neither of these fragments acted as effective dominant negatives (data not shown). As expected the C-terminal fragment did not co-immunoprecipitate with Rho1 while the GBD:FH3 protein did (Fig. 6). In addition to the co-immunoprecipitation experiments we also used the yeast two-hybrid system, but we did not detect an interaction between Rho1 and either Mwh or the GBD:FH3 protein. The reason for this is not clear. It is possible that the proteins do not directly interact or that the proteins when expressed in yeast are not competent to interact due to the need for a *Drosophila* specific third factor.

As an additional test of a possible *in vivo* interaction between Rho1 and either of the Mwh fragments we asked by immunostaining if these two proteins co-localized with Rho1. These experiments were done in a mwh^1 mutant background so the only Mwh protein present was the transgene encoded fragment. The GBD:FH3 fragment did not localize to growing hairs as did Rho1, but surprisingly we found that it accumulated on the proximal side of wing cells in a manner that mimicked Vang, Pk, In or Frtz (Figs. 7E, F — arrows). This accumulation appeared more tightly linked to the proximal side than endogenous full length Mwh, which is enriched proximally but is diffusely localized (Figs. 5C, D) (Strutt and Warrington, 2008; Yan et al., 2008). The ability of the GBD:FH3 protein to localize to the proximal side of wing cells, while it did not act as a dominant negative effects suggested that it might be possible to use this fragment to target other proteins to the proximal edge. The lack of co-localization with Rho1 was not surprising as only a small fraction of Rho1 was precipitated with Mwh. It is likely that most of the Rho1 immunostaining was to protein that was not interacting with Mwh. The C-terminal fragment did not preferentially localize to the proximal edge, but rather accumulated in growing hairs (Figs. 7A–C). Since we did not see any evidence for co-immunoprecipitation between Rho1 and Mwh-C, we do not think that the hair localization of Mwh-C was due to recruitment by Rho1.

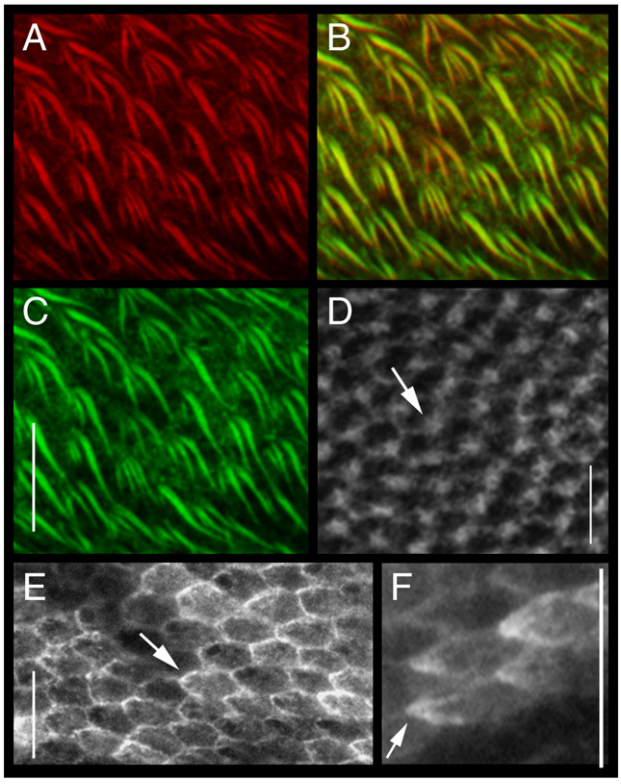

Fig. 7. The accumulation of Mwh in growing hairs is not due to a GBD:FH3 interaction. All imaged in this figure are oriented so that distal is to the right and proximal to the left. An *ap-Gal4/UAS-mwh-C*; mwh^1 pupal wing stained with anti-Mwh antibody (green) and with Alexa 568 phalloidin (red-F-actin) is shown (A–C). Note the strong multiple hair cell phenotype and abnormal hair polarity and that that Mwh-C protein accumulates in growing hairs similarly to the wild type Mwh. A younger wing prior to hair initiation (D) shows diffuse Mwh-C staining (arrow) on the side of the cell where hair formation is taking place. An *actin-Gal4/UAS-GBD:FH3-HA* wing stained with anti-HA antibody is shown at two different magnifications (EF). The uneven staining is due to the uneven expression that is often seen with this *actin-Gal4* driver. Note the uneven zigzag like accumulation on the proximal side of the cells (arrows).

Rho1 can alter the distribution of Core PCP proteins

The published data argued that Rho1 functioned downstream of the core PCP genes (Fanto et al., 2000; Strutt et al., 1997; Veeman et al., 2003). The range of Rho1 phenotypes we observed led us to suspect that this might not be so simple. As a test of this we examined the distribution of both Fz-GFP (this fusion protein is fully functional Strutt, 2001) and the endogenous Stan/Fmi protein in wings where a dominant negative or constitutively active Rho1 was expressed. We saw the zig zag staining of Fz-GFP was disrupted in cells where DN-Rho was expressed (Figs. 5E–J). As noted earlier in such wings the normal cell outline staining of DE-cadherin was disrupted in some cells and completely lost in others. In the disrupted cells there was substantial co-localization of DE-cadherin and Fz-GFP suggesting the possibility that the apical asymmetric accumulation of Fz is dependent on the presence of DE-cadherin in adherens junctions. We also examined the distribution of Fz-GFP in cells that expressed CA-Rho1 (Figs. 5K–P). As noted earlier this often results in gaps of DE-cadherin staining centered around tri-cellular junctions (Fig. 5P — arrowheads). The pattern of Fz-GFP accumulation was disrupted (Figs. 5K–P) but it was clear that there was not a 1 to 1 local correspondence between Fz-GFP and DE-cadherin (Fig. 5O — arrow).

The zig zag accumulation of Stan was also disrupted (and protein level decreased) in cells that expressed DN-Rho1 (Fig. 5C). Once again there were prominent gaps in Stan staining that were similar to that seen for Fz-GFP (arrowhead). We also localized Stan in wings that expressed a CA-Rho1 (Fig. 5D). The level of Stan staining appeared slightly increased and the zig zag pattern was disrupted, although not as severely as with DN-Rho1 (arrowheads). These epistasis experiments established that Rho1 functioned upstream of the core PCP genes. We suggest this is an indirect effect of Rho1's role in regulating cadherin accumulation and adherens junction formation/maintenance.

Discussion

Rho1 and tissue structure

We found that alterations in Rho1 activity had profound consequences for wing cell and tissue structure. These included changes in cell height and cross sectional area, apical hypertrophy and a loss of the simple one cell thick epithelial organization. Our results overlap but are somewhat different from those reported previously for the over expression of Rho1 in third instar wing discs, where it was reported that this led to cells losing apical basal polarity, leaving the epithelium basally and migrating between wild type cells (Speck et al., 2003). Perhaps the differences between the results were due to our cells only being exposed to a relatively short period of transgene expression and/or the different developmental stage. Our observations that both the expression of DN-Rho1 or enhanced RNAi knockdown of Rho1 led to shorter cells with greater cross section are opposite to results described in a recent paper where expression of DN-Rho1 was found to result in the elongation of wing disc cells (Widmann and Dahmann, 2009). The difference in the results may reflect tissue structure differences as third instar wing discs are highly folded while pupal wings are flat. They could also reflect differences in signal transduction pathways between the two developmental stages.

The expression of both dominant negative and constitutively active Rho1 led to a disruption in the lattice of adherens junctions that outline lateral–apical regions of pupal wing cells. These ranged from gaps in a still normally shaped lattice to a complete loss of staining in abnormally shaped and packed cells. The effects of DN-Rho1 were more severe and somewhat different in nature than for CA-Rho1. It is well known that E-Cadherin and Rho1 interact and there is a large literature that describes the activation of Rho1 by cadherin, however there is also evidence for Rho1 regulating Cadherin accumulation/intracellular trafficking (Fox et al., 2005; Magie et al., 2002; Xiao et al., 2007; Yamada and Nelson, 2007). We suggest that this is the basis for the effects of Rho1 mutations on Cadherin and the adherens junctions. Disruption of normal DE-cadherin staining and adherens junctions was also seen in cells that lacked Rap1 GTPase function (Knox and Brown, 2002). In that case DE-cadherin was enriched along specific cell–cell boundaries and gaps along individual borders were not seen as they are with Rho1. Although the two forms of Rho1 had relatively similar effects on DE-cadherin they had dramatically different effects on F-actin levels. The expression of DN-Rho1 led to a dramatic decrease in F-actin while in contrast the expression of CA-Rho1 increased peripheral F-actin. The effects of Rho1 on F-actin are consistent with its well-established regulation of the actin cytoskeleton. What is surprising is the uncoupling of adherens junctions and F-actin as these two components are normally tightly linked.

The activation of the cytoskeleton in wild type pupal wing cells results in the formation of a long and narrow cell extension (the prehair) that forms the cuticular hair. On the wing the hair emerges from a relatively flat cuticular surface. This general pattern of thin cuticular hairs is found over large regions of the adult *Drosophila*, but some body regions exhibit different sorts of cuticular structures. For example, a cuticle that contains prominent ridges with very small hairs covers much of the dorsal head capsule and the cuticle that lines the trachea is highly ridged and lacks hairs. Furthermore, a wide variety of cuticular structures and morphologies are found in other insects. In our experiments wing cells expressing CA-Rho had an extreme multiple hair cell phenotype that at early stages of hair differentiation resembled a ridge. This suggests that both developmental and evolutionary changes in the nature (e.g. ridge vs hair) and shape of cuticular structures could be mediated by changes in the pattern of small G protein activation.

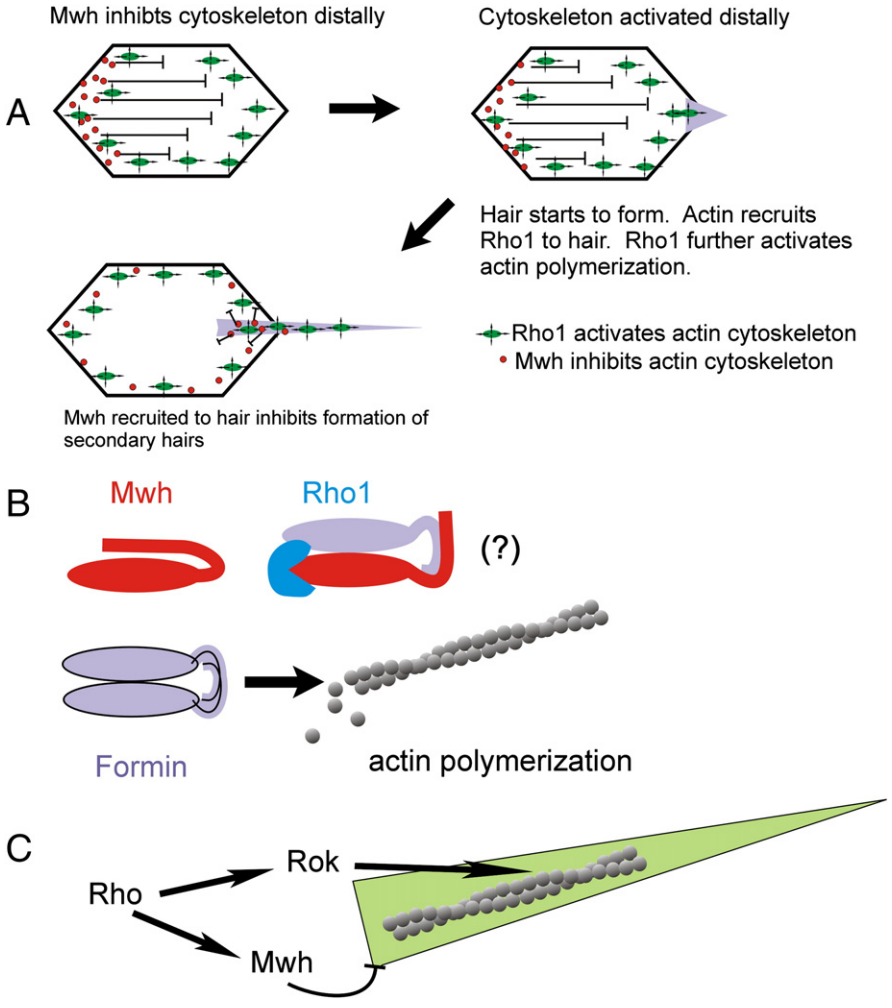

Fig. 8. Models for Rho1 and Mwh in planar polarity. Three stages in hair morphogenesis are shown in a cartoon form (A). Prior to hair initiation Rho1 is distributed widely in the cell and Mwh accumulates in the vicinity of the proximal edge. Rho1 activates the actin cytoskeleton while Mwh inhibits it. The distribution of these regulators leads to activation distally. Once hair extension begins F-actin in the hair recruits Rho1, which further stimulates actin polymerization. This positive feedback leads to robust hair growth. As the hair elongates Mwh is recruited to the proximal part of the hair where it inhibits the formation of new centers for actin polymerization. This insures a single hair is formed. A speculative model of how the Mwh–Rho1 interaction could regulate actin polymerization (B). By itself, Mwh cannot bind to a formin as its formin dimerization motif is hypothesized to be blocked by an autoinhibitory region. The binding of Rho1 to the GBD leads to a conformational change in Mwh and to the formin dimerization motif being exposed. This leads to the binding of a formin, but when paired with Mwh it cannot promote actin polymerization as it can when in a homodimer. Thus, Mwh is hypothesized to act as a "dominant negative" formin. Since there is no evidence for the ternary complex we have included a question mark. We hypothesize that Rho1 acts both positively (through the activation of Rok) and negatively (through the activation/stabilization of Mwh) in hair morphogenesis (C).

Does Rho1 bind the Mwh GBD?

In the diaphanous formins, Rho binding to the GBD results in a conformational change that activates the protein by moving an autoinhibitory segment (Goode and Eck, 2007; Rose et al., 2005). By analogy it was an attractive hypothesis that the binding of Rho1 to the Mwh GBD lead to a conformational change in Mwh that promoted its ability to inhibit hair initiation. For example, the movement of an autoinhibitory segment that allowed Mwh to bind to an effector protein. Candidates for such an effector would be formins as Mwh contains a potential formin dimerization segment. The binding of Mwh to a formin could block the formin from stimulating actin polymerization (Fig. 8B). Alternatively, the binding to Rho1 could have stabilized and/or locally recruited Mwh to a specific part of the cell. Consistent with such interactions mediating Mwh and Rho1 function in wing PCP we found that Mwh and Rho1 could be co-immunoprecipitated from wing disc cells, mutations in these two genes showed strong positive genetic interactions and that Mwh accumulation was promoted by Rho1 activity. Further, we found that Rho1 co-immunoprecipitated with the Mwh GBD-FH3 domain protein fragment from extracts of fly wing discs providing strong support for the GBD domain mediating the interaction between Rho1 and Mwh. The two proteins did not however show extensive co-localization prior to hair initiation; however, this may simply reflect a situation where only a small fraction of cellular Rho1 binds Mwh. This is consistent with our co-IP experiments and that Rho1 is known to interact with a variety of proteins. We saw more extensive co-localization in growing hairs however we do not think that this is mediated by an interaction between Rho1 and Mwh. The Mwh-C fragment accumulated in hairs but did not co-immunoprecipitate with Rho1, suggesting Mwh-C (and by extension Mwh) was recruited to the hair by an alternative mechanism.

Rho1 has mwh independent functions in wing planar polarity

We found that Rho1 and Rho1 regulators could modulate wing hair number in the absence of any *mwh* function. Hence, Rho1 must have a *mwh* independent function in hair morphogenesis. We suggest that this is mediated by Rho1 in growing hairs acting in parallel to activate Drok and hence the actin cytoskeleton (Fig. 8C). This is consistent with published data and the well-established role of Rho1 in activating Drok to regulate the actin cytoskeleton (Winter et al., 2001). Rho1 is known to have multiple effectors including ones that are thought to directly regulate the cytoskeleton and others that regulate transcription in the nucleus. We used Rho1 effector loop mutations to probe this issue and our results argue that the effects of Rho1 on cell shape and hair morphogenesis are largely if not entirely mediated through the cytoskeleton. Our results differ from those found in the eye for the role of Rho1 in planar polarity (Fanto et al., 2000), which we suspect is a consequence of the rather different cell biological basis for planar polarity in the wing and eye (Wong and Adler, 1993; Zheng et al., 1995).

The severe phenotypes obtained by the controlled expression of dominant negative or constitutively active Rho1 suggested that Rho1 mutations might also influence other parts of the planar polarity hierarchy. Indeed, we found that the normal zig zag accumulation pattern of Fz and Stan proteins (and presumably other core PCP proteins as these appear to be a functional unit) could be disrupted by such treatments. One interpretation of this is that Rho1 functions directly upstream of the core PCP proteins. For example, Rho1 activity might regulate the expression of one or more of the PCP genes (e.g. Lee and Adler, 2004) or that Rho1 might directly mediate the intracellular transport of PCP proteins (Shimada et al., 2006). An alternative hypothesis is that the gross alterations in cell shape and cytoskeleton function associated with alterations in Rho1 function indirectly altered the subcellular distribution of PCP proteins. Of particular note was the loss of and gaps in DE-cadherin staining (and presumably AJs). Cells that showed a disruption in DE-cadherin distribution also showed a disruption in Fz and Stan accumulation. The cellular and molecular basis for this is unclear. It is known that PCP proteins accumulate at the level of the AJ and that the proper accumulation of Fz requires normal cell apical basal polarity (Djiane et al., 2005). It is possible that direct interactions between AJ components and one or more of the PCP proteins is essential for the recruitment or stability of PCP protein complexes. Djiane et al. (2005) reported a direct interaction between Fz and the apically localized dPatj protein, although this was not required for proper Fz localization. In other contexts it has been found that the cytoplasmic domain of some Cadherins can bind PDZ domains directly (Boeda et al., 2002; Demontis et al., 2006; Siemens et al., 2002) and other Cadherins (such as DE-cadherin) can interact with PDZ domains indirectly by virtue of their interaction with catenins (Demontis et al., 2006; Itoh et al., 1999; Perego et al., 2000). Several proteins involved in PCP contain PDZ domains (e.g. Dsh, In and Kermit) and these could mediate/stabilize interactions between E-cadherin/catenin and PCP protein complexes. The expression of DN and CA Rho1 also had profound affects on the actin cytoskeleton and in recent years it has been found that the actin cytoskeleton is not only a target of the Fz pathway but its function is also required for the development of normal PCP and the establishment of the proximal and distal PCP protein complexes (Blair et al., 2006; Ren et al., 2007). This provides an alternative mechanism by which Rho1 mutations could indirectly interfere with normal PCP.

A model for Rho1 in wing tissue polarity

In our experiments we found that Rho1 accumulated in growing hairs where it would be positioned to activate the actin cytoskeleton for hair morphogenesis. Prior to hair morphogenesis complexes of PCP, PPE and Mwh proteins accumulated on either the distal or proximal sides of wing cells. At this time Rho1 was widely distributed and we suggest it functioned to insure the normal lattice of adherens junctions, which our experiments argued was needed for the formation of the distal and proximal PCP protein complexes. Rho1 also promoted the accumulation of Mwh. As wing differentiation proceeds we expect that there is an accumulation of proteins that can activate the cytoskeleton. Mwh located on the proximal side could act locally to inhibit the cytoskeleton leading to hair initiation centers forming far from Mwh — on the distal side of wing cells (Fig. 8A). When the levels of activators increased above a threshold the cytoskeleton would be activated on the distal side of the cell and hair formation would begin. As part of this process Rho1 would be recruited, which would in turn activate Rho kinase. This would lead to the further activation of the cytoskeleton and further recruitment of Rho1. This positive feedback system would lead to vigorous hair morphogenesis and vigorous refinement. Our data suggested that Rho1 also has a second function to recruit/activate/stabilize Mwh to insure that no secondary initiation sites form (Yan et al., 2008). Thus, Rho1 would function as both a positive and negative regulator of hair morphogenesis (Fig. 8C). This dual function, in addition to the role of Rho1 in maintaining cell structure, would lead to the wide range of mutant phenotypes seen in Rho1 mutants.

Acknowledgments

This work was supported by a grant from the NIGMS to pna. We thank Jeannette Charlton for help with some of the experiments. We thank our colleagues in the fly community for generously sharing reagents.

Appendix A. Supplementary data

Supplementary data associated with this article can be found, in the online version, at doi:10.1016/j.ydbio.2009.06.027.

References

Adler, P.N., 2002. Planar signaling and morphogenesis in *Drosophila*. Dev. Cell 2, 525–535.

Adler, P.N., Zhu, C., Stone, D., 2000. Cell size and the morphogenesis of epidermal hairs. Genesis 28, 82–91.

Adler, P.N., Liu, J., Charlton, J., 2004. Inturned localizes to the proximal side of wing cells under the instruction of upstream planar polarity proteins. Curr. Biol. 14, 2046–2051.

Axelrod, J.D., 2001. Unipolar membrane association of Dishevelled mediates Frizzled planar cell polarity signaling. Genes Dev. 15, 1182–1187.

Bastock, R., Strutt, H., Strutt, D., 2003. Strabismus is asymmetrically localised and binds to Prickle and Dishevelled during *Drosophila* planar polarity patterning. Development 130, 3007–3014.

Billuart, P., Winter, C.G., Maresh, A., Zhao, X., Luo, L., 2001. Regulating axon branch stability: the role of p190 RhoGAP in repressing a retraction signaling pathway. Cell 107, 195–207.

Blair, A., Tomlinson, A., Pham, H., Gunsalus, K.C., Goldberg, M.L., Laski, F.A., 2006. Twinstar, the *Drosophila* homolog of cofilin/ADF, is required for planar cell polarity patterning. Development 133, 1789–1797.

Boeda, B., El-Amraoui, A., Bahloul, A., Goodyear, R., Daviet, L., Blanchard, S., Perfettini, I., Fath, K.R., Shorte, S., Reiners, J., Houdusse, A., Legrain, P., Wolfrum, U., Richardson, G., Petit, C., 2002. Myosin VIIa, harmonin and cadherin 23, three Usher I gene products that cooperate to shape the sensory hair cell bundle. EMBO J. 21, 6689–6699.

Buenzow, D.E., Holmgren, R., 1995. Expression of the *Drosophila* gooseberry locus defines a subset of neuroblast lineages in the central nervous system. Dev. Biol. 170, 338–349.

Chae, J., Kim, M.J., Goo, J.H., Collier, S., Gubb, D., Charlton, J., Adler, P.N., Park, W.J., 1999. The *Drosophila* tissue polarity gene starry night encodes a member of the protocadherin family. Development 126, 5421–5429.

Collier, S., Gubb, D., 1997. *Drosophila* tissue polarity requires the cell-autonomous activity of the fuzzy gene, which encodes a novel transmembrane protein. Development 124, 4029–4037.

Collier, S., Lee, H., Burgess, R., Adler, P., 2005. The WD40 repeat protein fritz links cytoskeletal planar polarity to frizzled subcellular localization in the *Drosophila* epidermis. Genetics 169, 2035–2045.

Cong, J., Geng, W., He, B., Liu, J., Charlton, J., Adler, P., 2001. The furry gene of *Drosophila* is important for maintaining the integrity of cellular extensions during morphogenesis. Development 128, 2793–2802.

Demontis, F., Habermann, B., Dahmann, C., 2006. PDZ-domain-binding sites are common among cadherins. Dev. Genes Evol. 216, 737–741.

Dietzl, G., Chen, D., Schnorrer, F., Su, K.C., Barinova, Y., Fellner, M., Gasser, B., Kinsey, K., Oppel, S., Scheiblauer, S., Couto, A., Marra, V., Keleman, K., Dickson, B.J., 2007. A genome-wide transgenic RNAi library for conditional gene inactivation in *Drosophila*. Nature 448, 151–156.

Djiane, A., Yogev, S., Mlodzik, M., 2005. The apical determinants aPKC and dPatj regulate Frizzled-dependent planar cell polarity in the *Drosophila* eye. Cell 121, 621–631.

Fanto, M., Weber, U., Strutt, D.I., Mlodzik, M., 2000. Nuclear signaling by Rac and Rho GTPases is required in the establishment of epithelial planar polarity in the *Drosophila* eye. Curr. Biol. 10, 979–988.

Feiguin, F., Hannus, M., Mlodzik, M., Eaton, S., 2001. The ankyrin repeat protein Diego mediates Frizzled-dependent planar polarization. Dev. Cell 1, 93–101.

Fox, D.T., Homem, C.C., Myster, S.H., Wang, F., Bain, E.E., Peifer, M., 2005. Rho1 regulates *Drosophila* adherens junctions independently of p120ctn. Development 132, 4819–4831.

Geng, W., He, B., Wang, M., Adler, P.N., 2000. The tricornered gene, which is required for the integrity of epidermal cell extensions, encodes the *Drosophila* nuclear DBF2-related kinase. Genetics 156, 1817–1828.

Goode, B.L., Eck, M.J., 2007. Mechanisms and function of formins in the control of actin assembly. Ann. Rev. Biochem. 76, 593–627.

Gregory, S.L., Shandala, T., O'Keefe, L., Jones, L., Murray, M.J., Saint, R., 2007. A *Drosophila* overexpression screen for modifiers of Rho signalling in cytokinesis. Fly (Austin) 1, 13–22.

Gubb, D., Green, C., Huen, D., Coulson, D., Johnson, G., Tree, D., Collier, S., Roote, J., 1999. The balance between isoforms of the prickle LIM domain protein is critical for planar polarity in *Drosophila* imaginal discs. Genes Dev. 13, 2315–2327.

Gumbiner, B.M., 2005. Regulation of cadherin-mediated adhesion in morphogenesis. Nat. Rev. Mol. Cell Biol. 6, 622–634.

He, Y., Fang, X., Emoto, K., Jan, Y.N., Adler, P.N., 2005. The tricornered Ser/Thr protein kinase is regulated by phosphorylation and interacts with furry during *Drosophila* wing hair development. Mol. Biol. Cell 16, 689–700.

Hickson, G.R., O'Farrell, P.H., 2008. Rho-dependent control of anillin behavior during cytokinesis. J. Cell. Biol. 180, 285–294.

Itoh, M., Morita, K., Tsukita, S., 1999. Characterization of ZO-2 as a MAGUK family member associated with tight as well as adherens junctions with a binding affinity to occludin and alpha catenin. J. Biol. Chem. 274, 5981–5986.

Jenny, A., Darken, R.S., Wilson, P.A., Mlodzik, M., 2003. Prickle and Strabismus form a functional complex to generate a correct axis during planar cell polarity signaling. EMBO J. 22, 4409–4420.

Kiehart, D.P., Franke, J.D., Chee, M.K., Montague, R.A., Chen, T.L., Roote, J., Ashburner, M., 2004. *Drosophila* crinkled, mutations of which disrupt morphogenesis and cause lethality, encodes fly myosin VIIA. Genetics 168, 1337–1352.

Knox, A.L., Brown, N.H., 2002. Rap1 GTPase regulation of adherens junction positioning and cell adhesion. Science 295, 1285–1288.

Lamb, R.S., Ward, R.E., Schweizer, L., Fehon, R.G., 1998. *Drosophila* coracle, a member of the protein 4.1 superfamily, has essential structural functions in the septate junctions and developmental functions in embryonic and adult epithelial cells. Mol. Biol. Cell 9, 3505–3519.

Lawrence, P.A., Struhl, G., Casal, J., 2007. Planar cell polarity: one or two pathways? Nat. Rev. Genet. 8, 555–563.

Lee, H., Adler, P.N., 2004. The grainy head transcription factor is essential for the function of the frizzled pathway in the *Drosophila* wing. Mech. Dev. 121, 37–49.

Magie, C.R., Pinto-Santini, D., Parkhurst, S.M., 2002. Rho1 interacts with p120ctn and alpha-catenin, and regulates cadherin-based adherens junction components in *Drosophila*. Development 129, 3771–3782.

McGuire, S.E., Le, P.T., Osborn, A.J., Matsumoto, K., Davis, R.L., 2003. Spatiotemporal rescue of memory dysfunction in *Drosophila*. Science 302, 1765–1768.

Montcouquiol, M., 2007. [Planar polarity in mammals: similarity and divergence with *Drosophila melanosgaster*]. J. Soc. Biol. 201, 61–67.

Narumiya, S., Yasuda, S., 2006. Rho GTPases in animal cell mitosis. Curr. Opin. Cell Biol. 18, 199–205.

Ng, J., Luo, L., 2004. Rho GTPases regulate axon growth through convergent and divergent signaling pathways. Neuron 44, 779–793.

Oda, H., Uemura, T., Harada, Y., Iwai, Y., Takeichi, M., 1994. A *Drosophila* homolog of cadherin associated with armadillo and essential for embryonic cell–cell adhesion. Dev Biol 165, 716–726.

Park, W., Liu, J., Sharp, E., Adler, P., 1996. The *Drosophila* tissue polarity gene inturned acts cell autonomously and encodes a novel protein. Development 122, 961–969.

Perego, C., Vanoni, C., Massari, S., Longhi, R., Pietrini, G., 2000. Mammalian LIN-7 PDZ proteins associate with beta-catenin at the cell–cell junctions of epithelia and neurons. EMBO J. 19, 3978–3989.

Prokopenko, S.N., Brumby, A., O'Keefe, L., Prior, L., He, Y., Saint, R., Bellen, H.J., 1999. A putative exchange factor for Rho1 GTPase is required for initiation of cytokinesis in *Drosophila*. Genes Dev. 13, 2301–2314.

Ren, N., Charlton, J., Adler, P.N., 2007. The flare gene, which encodes the AIP1 protein of *Drosophila*, functions to regulate F-actin disassembly in pupal epidermal cells. Genetics 176, 2223–2234.

Rivero, F., Muramoto, T., Meyer, A.K., Urushihara, H., Uyeda, T., Kitayama, C., 2005. A comparative sequence analysis reveals a common GBD/FH3-FH1-FH2-DAD architecture in formins from Dictyostelium, fungi and metazoa. BMC Genomics 6, 28.

Rose, R., Weyand, M., Lammers, M., Ishizaki, T., Ahmadian, M.R., Wittinghofer, A., 2005. Structural and mechanistic insights into the interaction between Rho and mammalian Dia. Nature 435, 513–518.

Sahai, E., Alberts, A.S., Treisman, R., 1998. RhoA effector mutants reveal distinct effector pathways for cytoskeletal reorganization, SRF activation and transformation. EMBO J. 17, 1350–1361.

Shimada, Y., Usui, T., Yanagawa, S.-i., Takeichi, M., Uemura, T., 2001. Asymmetric colocalization of Flamingo, a seven-pass transmembrane cadherin, and Dishevelled in planar cell polarization. Curr. Biol. 11, 859–863.

Shimada, Y., Yonemura, S., Ohkura, H., Strutt, D., Uemura, T., 2006. Polarized transport of frizzled along the planar microtubule arrays in *Drosophila* wing epithelium. Dev. Cell 10, 209–222.

Siemens, J., Kazmierczak, P., Reynolds, A., Sticker, M., Littlewood-Evans, A., Muller, U., 2002. The Usher syndrome proteins cadherin 23 and harmonin form a complex by means of PDZ-domain interactions. Proc. Natl. Acad. Sci. U. S. A. 99, 14946–14951.

Speck, O., Hughes, S.C., Noren, N.K., Kulikauskas, R.M., Fehon, R.G., 2003. Moesin functions antagonistically to the Rho pathway to maintain epithelial integrity. Nature 421, 83–87.

Struhl, G., Basler, K., 1993. Organizing activity of wingless protein in *Drosophila*. Cell 72, 527–540.

Strutt, D.I., 2001. Asymmetric localization of frizzled and the establishment of cell polarity in the *Drosophila* wing. Mol. Cell 7, 367–375.

Strutt, D., Warrington, S.J., 2008. Planar polarity genes in the *Drosophila* wing regulate the localisation of the FH3-domain protein Multiple Wing Hairs to control the site of hair production. Development 135, 3103–3111.

Strutt, D.I., Weber, U., Mlodzik, M., 1997. The role of RhoA in tissue polarity and Frizzled signalling. Nature 387, 292–295.

Tree, D.R.P., Shulman, J.M., Rousset, R., Scott, M.P., Gubb, D., Axelrod, J.D., 2002. Prickle mediates feedback amplification to generate asymmetric planar cell polarity signaling. Cell 109, 371–381.

Turner, C.M., Adler, P.N., 1998. Distinct roles for the actin and microtubule cytoskeletons in the morphogenesis of epidermal hairs during wing development in *Drosophila*. Mech. Dev. 70, 181–192.

Usui, T., Shima, Y., Shimada, Y., Hirano, S., Burgess, R.W., Schwarz, T.L., Takeichi, M., Uemura, T., 1999. Flamingo, a seven-pass transmembrane cadherin, regulates planar cell polarity under the control of frizzled. Cell 98, 585–595.

Van Aelst, L., Symons, M., 2002. Role of Rho family GTPases in epithelial morphogenesis. Genes Dev. 16, 1032–1054.

Veeman, M.T., Axelrod, J.D., Moon, R.T., 2003. A second canon. Functions and mechanisms of beta-catenin-independent Wnt signaling. Dev. Cell 5, 367–377.

Vinson, C.R., Conover, S., Adler, P.N., 1989. A *Drosophila* tissue polarity locus encodes a protein containing seven potential transmembrane domains. Nature 338, 263–264.

Wang, Y., Nathans, J., 2007. Tissue/planar cell polarity in vertebrates: new insights and new questions. Development 134, 647–658.

Widmann, T.J., Dahmann, C., 2009. Dpp signalling promotes the cuboidal to collumnar shape transition of *Drosophila* wing disc epithelia by regulating RHo1. J. Cell Sci. 122, 1362–1373.

Winter, C.G., Wang, B., Ballew, A., Royou, A., Karess, R., Axelrod, J.D., Luo, L., 2001. *Drosophila* rho-associated kinase (drok) links frizzled-mediated planar cell polarity signaling to the actin cytoskeleton. Cell 105, 81–91.

Wolff, T., Rubin, G., 1998. Strabismus, a novel gene that regulates tissue polarity and cell fate decisions in *Drosophila*. Development 125, 1149–1159.
Wong, L., Adler, P., 1993. Tissue polarity genes of *Drosophila* regulate the subcellular location for prehair initiation in pupal wing cells. J. Cell Biol. 123, 209–221.
Woods, D.F., Bryant, P.J., 1991. The discs-large tumor suppressor gene of *Drosophila* encodes a guanylate kinase homolog localized at septate junctions. Cell 66, 451–464.
Xiao, K., Oas, R.G., Chaisson, C.M., Kowalczyk, A.P., 2007. Role of p120-catenin in cadherin trafficking. Biochim. Biophys Acta 1773, 8–16.
Yamada, S., Nelson, W.J., 2007. Localized zones of Rho and Rac activities drive initiation and expansion of epithelial cell–cell adhesion. J. Cell Biol. 178, 517–527.
Yan, J., Huen, D., Morely, T., Johnson, G., Gubb, D., Roote, J., Adler, P.N., 2008. The multiple-wing-hairs gene encodes a novel GBD-FH3 domain-containing protein that functions both prior to and after wing hair initiation. Genetics 180, 219–228.
Zallen, J.A., 2007. Planar polarity and tissue morphogenesis. Cell 129, 1051–1063.
Zheng, L., Zhang, J., Carthew, R.W., 1995. frizzled regulates mirror-symmetric pattern formation in the *Drosophila* eye. Development 121, 3045–3055.
Zohar, M., Teramoto, H., Katz, B.Z., Yamada, K.M., Gutkind, J.S., 1998. Effector domain mutants of Rho dissociate cytoskeletal changes from nuclear signaling and cellular transformation. Oncogene 17, 991–998.